NIH Public Access
Author Manuscript
Proteomics. Author manuscript; available in PMC 2015 April 01.

Published in final edited form as:
Proteomics. 2014 April ; 14(0): 936–944. doi:10.1002/pmic.201300406.

The utilization of fluorescence to identify the components of lipofuscin by imaging mass spectrometry

Zsolt Ablonczy[1,*], **Noah Smith**[2], **David M Anderson**[3], **Angus C. Grey**[4], **Jeffrey Spraggins**[3], **Yiannis Koutalos**[1], **Kevin L. Schey**[3], and **Rosalie K. Crouch**[1]

[1]Department of Ophthalmology, Medical University of South Carolina, Charleston, SC 29425

[2]Clemson University, Clemson, SC 29634

[3]Department of Biochemistry, Vanderbilt University School of Medicine, Nashville, TN 37240

[4]Department of Physiology, University of Auckland, Auckland, New Zealand, 1023

Abstract

Lipofuscin, an aging marker in the retinal pigment epithelium (RPE) associated with the development of age-related macular degeneration, is primarily characterized by its fluorescence. The most abundant component of RPE lipofuscin is N-retinylidene-N-retinylethanolamine (A2E) but its exact composition is not known due to the complexity of the RPE extract. In this study, we utilized MALDI imaging to find potential molecules responsible for lipofuscin fluorescence in RPE tissue from *Abca4*$^{-/-}$, *Sv129*, and *C57Bl6/J* mice ages 2 and 6 month. To assert relationships, the individual images in the MALDI imaging datasets were correlated with lipofuscin fluorescence recorded from the same tissues following proper registration. Spatial correlation information, which is usually is lost in bioanalytics, pinpointed a relatively small number of potential lipofuscin components. The comparison of four samples in each condition further limited the possibility of false positives and provided various new, age- and strain-specific targets. Validating the usefulness of the fluorescence-enhanced imaging strategy, many known adducts of A2E were identified in the short list of lipofuscin components. These results provided evidence that mass spectrometric imaging can be utilized as a tool to begin to identify the molecular substructure of clinically-relevant diagnostic information.

Keywords

lipofuscin; A2E; MALDI imaging; RPE; mouse

1. Introduction

Lipofuscin, a widely used term for undegraded fluorescent lysosomal waste, is gradually accumulating with age in the cells of the central nervous system and most major organs [1]. Thus, in addition to being a convenient marker for aging, lipofuscin is often implicated in

*Corresponding author: Zsolt Ablonczy, Ph.D., Medical University of South Carolina, Storm Eye Institute, Rm 518E, 167 Ashley Ave., Charleston, SC 29425. Tel: 843-792-0777; Fax: 843-792-1723; ablonczy@musc.edu.

The authors have declared no conflict of interest.

NIH-PA Author Manuscript
NIH-PA Author Manuscript
NIH-PA Author Manuscript

NIH-PA Author Manuscript

NIH-PA Author Manuscript

NIH-PA Author Manuscript

both normal aging processes and diverse age-related pathologies [2–5]. In the eye, lipofuscin is primarily found in the cells of the RPE [6–8] and can be detected as early as one year of age [6] with signals increasing over the years [7]. Lipofuscin fluorescence is highest in the posterior pole of the RPE [7], the area where age-related macular degeneration (AMD) lesions usually develop, and therefore, it is often measured clinically using common ophthalmic diagnostic instrumentation. When extracted from the native tissue, the fluorescent lipofuscin granules have been shown to exhibit toxicity to cultured RPE cells [9–11], thereby linking lipofuscin fluorescence to AMD, a principal cause of incurable vision loss worldwide [12, 13].

The toxic component in RPE lipofuscin, however, has not been identified. The proteomics study by Ng et al. on human RPE lipofuscin granules shows a complex mixture of lipids and protein components, but with less than 2% of the material by weight containing amino acids [14]. As analytical efforts have long been hindered by the insolubility of the material, it is estimated that up to half of the total lipofuscin content is still unknown [12, 14]. Although its composition is not fully understood in any tissues, the lipofuscin in the RPE is known to be enriched in pyridinium *bis*-retinoids [15, 16], which have a broad fluorescence emission spectrum similar to RPE lipofuscin [26]. The most abundant *bis*-retinoid is the amphoteric quaternary amine, N-retinylidene-N-retinylethanolamine (A2E). The precursor of A2E, A2PE, forms in the photoreceptors from retinaldehydes [17–19] and phosphatidyl-ethanolamine and is internalized by the RPE through phagocytosis, wherein they are partially degraded into A2E [17–21]. For an overview of these reactions, see Figure 1. The accumulation of A2E is accelerated in Stargardt disease, a juvenile form of macular degeneration [22], and numerous studies have suggested a detrimental role for A2E in AMD development (see reviewed in [15]). On the other hand, additional studies indicated that A2E may be less damaging than retinaldehydes [23, 24]. Nevertheless, these experiments (based on organic extracts of whole RPE tissues) prevent any spatial correlation to the characteristic fluorescence itself. To clarify the role of A2E and other related *bis*-retinoids in age-related RPE toxicity, independent forms of validation are required using spatial methods comparable to fluorescence.

Since traditional immuno-localization techniques are not applicable, to achieve molecular specificity at a high spatial resolution we have developed a MALDI imaging mass spectrometry-based technique. Our previous studies demonstrated high spatial correlation between A2E and the fluorescence of lipofuscin in the mouse [25, 26]. To begin to comprehensively understand the composition of lipofuscin, recently, we have established a fluorescence-enhanced imaging strategy, which allows the utilization of spatial information encoded in the MALDI imaging datasets [27]. To limit the possibility of false positives inherent with the above methods, here we present the results of a comprehensive analysis of lipofuscin composition in four eyes each from *Abca4*$^{-/-}$ (a model of Stargardt disease), *Sv129* (the base strain for *Abca4*$^{-/-}$ mice), and another commonly used model, *C57Bl6/J* mice. To probe the effect of aging, two and six month old animals were utilized. Our results show that the unique spatial information in the MALDI imaging datasets can be utilized as a tool for a fast and efficient survey of the relevant molecular substructure of diagnostic information. These studies validated decades of previous work on the composition of

NIH-PA Author Manuscript

NIH-PA Author Manuscript

NIH-PA Author Manuscript

lipofuscin and allowed the identification of new, age- and strain-specific molecular markers of lipofuscin by a thorough the comparative mathematical analysis of the MALDI imaging data.

2. Materials and methods

2.1. Animal tissues

All animal work was designed and performed in accordance with the ARVO (Association for Research in Vision and Ophthalmology) Statement for the Use of Animals in Ophthalmic and Vision Research and protocols were approved by the Medical University of South Carolina Animal Care and Use Committee. *C57Bl6/J* and *Sv129* mice were obtained from Harlan Laboratories (Indianapolis, IN), breeding pairs for *Abca4*$^{-/-}$ mice were a generous gift from Dr. Gabriel Travis (UCLA, Los Angeles). Procedures for the murine eye tissue preparation have been reported previously [25]. In short, four eyes from freshly euthanized 2 or 6 month old animals were enucleated and desiccated under dim red light, the anterior part and neural retina was removed and eyecup tissues were carefully flat-mounted with their scleral-side down on indium tin oxide-coated conductive glass slides (Delta Technologies Ltd, Stillwater, MN) to preserve the original orientation.

2.2. Fluorescence imaging

Fluorescence images of overlapping fields were collected on an 8-bit absolute intensity scale using the SP2-RS Laser Scanning Confocal Microscope (Leica, Wetzlar, Germany) and assembled to provide a single image of the entire eyecup as detailed previously [25]. To eliminate any background fluorescence, contrast has been adjusted using the Image-J software (NIH, Bethesda, MD) equally for each fluorescent image. For the image shown, pixel intensities were plotted on a color scale (0 – 100: red ~ 90, orange ~ 80, ~ yellow ~ 70, green ~ 50, light blue ~ 30, and dark blue ~ 15).

2.3. MALDI imaging

The mouse tissue was prepared for MALDI imaging by automated matrix deposition (Portrait 630; Labcyte, Sunnyvale, CA) with 10 mg/mL 2′,5′-dihydroxyacetophenone (Sigma Chemical Co, St Loius, MO) in 70:30 ethanol (Thermo Fisher, Waltham, MA):water (v:v) with a final center-to-center spot distance of 150 μm. MALDI data were collected on an Ultraflextreme TOF mass spectrometer (Bruker, Billerica, MA) in the m/z 420 – 1400 range, with a raster step size of 150 μm. Additional technical details were published previously [25]. The instrument collects images over the entire tissue surface in the selected m/z range. In the observed m/z range of 420–1400 this corresponded to 8000 linear data points or m/z bins. MALDI images were reconstructed from these data using the FlexImaging 2.0 software (Bruker) and plotted in a mass window consisting of ± 0.5 m/z units around the mass of interest (integrating data from roughly 8 individual data points for each image). For display purposes, data were normalized to total ion current, interpolated, and pixel intensities for all data sets plotted on the same color scale described above for “Fluorescence imaging”. Given the resolution of the instrument and sample to sample variation in mass calibration, the mass accuracy of the various samples was 0.1–0.3 amu, therefore, mass values shown to be rounded to one decimal digit.

NIH-PA Author Manuscript

NIH-PA Author Manuscript

NIH-PA Author Manuscript

MS/MS analysis was performed using a 9.4T Bruker SolariX FTICR mass spectrometer (Bruker Daltonics, Billerica, MA, USA). The precursor ion mass was selected in the source region of the instrument using a linear quadrupole (m/z window: 1.0 Da). The selected ions were fragmented by SORI CID [28] (pulsed argon, 0.25s 500Hz irradiation). MS/MS spectra were processed and figures generated using DataAnalysis (Bruker).

2.4. Correlation of lipofuscin with the molecules in the imaging dataset

Details of this strategy have been described elsewhere [27]. In short, for each tissue the intensity profiles for all 8000 individually collected m/z bins were exported into Analyze 7.5 format stacks of images on an 8-bit absolute intensity scale without interpolation. To calculate the correlation coefficients between the image of lipofuscin fluorescence and each individual image in the stack, the lipofuscin fluorescence image was registered (stretched and rotated) to overlap by visual observation, recomposed into a number of squares corresponding to the resolution of the MALDI images using pixel averaging and finally re-scaled to match the resolution of the MALDI images. The similarity between the resultant fluorescence image and each of the individual images in the MALDI imaging data stack was quantitated by calculating pairwise Pearson correlation coefficients using Image-J. Correlation coefficients were plotted against the m/z values of the corresponding data points in the MALDI imaging dataset.

3. Results

3.1. Visual correlation of lipofuscin and A2E in Abca4$^{-/-}$ mice

One of the preeminent advantages of imaging mass spectrometry is that it allows the comparison of images obtained with traditional imaging modalities with molecularly specific spatial data. This is usually performed by comparing consecutive histological sections with the MALDI data. In our fluorescence-enhanced imaging strategy, to minimize sample manipulations autofluorescence images of lipofuscin are first collected in a fluorescent microscope and then the same tissue is spot-coated with MALDI matrix for mass spectrometric imaging (IMS) analysis. The results of these experiments are briefly summarized in Figure 2, Supplementary Figure 1, and Supplementary Figure 2.

Fig. 2A contains the fluorescent image of lipofuscin from a six month old *Abca4*$^{-/-}$ mouse and Fig. 2B is the corresponding MALDI image of A2E in the same tissue. These micrographs represent the images with the original resolution recorded using the laser scanning microscope and the interpolated image exported from Fleximaging. For a direct comparison of lipofuscin with A2E is used in the subsequent correlation analysis, the panels are shown using the pixel resolution of the exported Analyze 7.5 MALDI imaging data cube. Supplementary Fig. 1A and 1B represent the same panels but with the higher resolution of the microscope camera and the same MALDI images interpolated. These images provide convincing evidence that, in this particular tissue, lipofuscin and A2E distributions correlate visually. To further validate the visual correlations, Supplementary Fig. 2A and 2B show the cross sectional profiles over the tissues as indicated in Supplementary Fig. 1.

NIH-PA Author Manuscript

NIH-PA Author Manuscript

NIH-PA Author Manuscript

3.2. A limited set of molecules correlate with lipofuscin fluorescence in Abca4$^{-/-}$ mice

The MALDI imaging dataset with its 8000 consecutive individual images (one for each m/z bin) allows a unique opportunity to establish spatial correlation between lipofuscin and any m/z value in the image stack [27]. The results of this analysis for the same tissue (6 month old *Abca4*$^{-/-}$ mouse) as used above are summarized in Figure 3 using the MALDI imaging dataset. Fig. 3A shows the average MALDI mass spectrum in the m/z 500–1300 range. A2E (m/z 592.4) is clearly observable as the base peak in this mass spectrum and its singly oxidized version (A2E+ox, m/z 608.4) is also detected well above background. However, additional A2E-related ions were not detected beyond the background noise in the average MALDI mass spectrum. Fig. 3B charts the correlation coefficients between lipofuscin and the individual images in the stack against the m/z values corresponding to those images. In this representation, A2E itself shows the highest correlation coefficient reflecting its highly similar spatial distribution to lipofuscin. However, this analysis also shows several other ions with correlation values similar to A2E. In fact, the m/z values corresponding to these peaks coincide with a series of known A2E-related molecules. These potentially highly correlating peaks are of low abundance and visibly indistinguishable from the background in the average MALDI mass spectrum (Fig. 3A) but they are detected by the correlation analysis as they are slightly above baseline in some particular areas over the entire surface, where A2E is also present.

Table 1 summarizes the results of the correlation analysis for the most abundant ions in the sample. Only the monoisotopic m/z ratios are listed. The histogram of the correlation coefficient values (Fig. 3C) can be approximated well as the sum of two Gaussian distributions. The Gaussian noise (−0.094±0.11) and the correlations associated with the data (0.39±0.13) were distinct, essentially with any correlation coefficient value > 0.3 being significantly distinct from noise ($p<0.01$). Within the correlations associated with the data, coefficients > 0.65 can be considered statistically different from the mean ($p<0.05$). The correlation analysis for the ions in Tab. 1 provided linear correlation plots with limited scattering (see Supplementary Figure 3 for the ions represented in Fig. 2).

The majority of peaks listed in Tab. 1 are consistent with being potential A2E-related compounds: A2E and its oxides (for the distributions, see Figs. 2B–2D), pospho-A2E (m/z 673.3, see in Fig. 2E) and its oxides, A2-GPE (m/z 746.2, see in Fig. 2F) and its oxides. Tandem mass spectrometry has confirmed the identity of these peaks by similarity to spectra published [25, 29], for comparison with m/z 746.2 see Supplementary Fig. 4A. There were in the list, however, other prominent ions as well (m/z 634.4, m/z 650.4, m/z 787.6, and m/z 816.0) the molecular weight of which are not consistent with known modifications of A2E. The apparent correlation values, the high separation from noise, and the linear correlation plots of these ions made them equally as significant as some of the known A2E-related compounds. The spatial distributions of these ions across the RPE are shown in Figures 2G–2J.

The molecules with m/z values close to A2E (m/z 634.4, m/z 650.4) are of particular interest, as they may be novel A2E-related compounds with comparatively simple chemical modifications. The molecular weight shift of +16 amu between the two ions is consiustent

NIH-PA Author Manuscript

NIH-PA Author Manuscript

NIH-PA Author Manuscript

with the addition of an oxygen on the same base compound. Although a + 42 amu shift could be considered acetylation for m/z 634.4, MS/MS data collected (Supplementary Fig. 4B) provides evidence of a fragment that corresponds to singly-oxidized A2E (m/z 608.5) and several other fragments that reflect losses characteristic to A2E (+151 and +174 for peaks m/z 483.0 and 460.9 respectively, compare to [30]). The molecular weight difference of +26 amu of m/z 634.4 compared to m/z 608 being consistent with formylation identifies m/z 634.4 as singly-oxidized and formylated A2E rather than A2E acetyl ester, and m/z 650.4 as doubly-oxidized and formylated A2E.

3.3. Age- and strain-specific molecules in mouse lipofuscin

To identify changes in lipofuscin composition in *Abca4*$^{-/-}$ mice due to the particular genetic background and to test the presence of false positives represented in a particular sample, we have similarly analyzed four eyes each from non-littermate two and six month old *Abca4*$^{-/-}$ and *Sv129* mice and from two 6 month old *C57Bl6/J* mice. The obtained results are summarized in Table 2. To eliminate inaccuracy arising from directly comparing correlation coefficients, which can deviate significantly between individual samples, a rank-based strategy was utilized to summarize the data. The 20 highest correlating ions were ranked from 1 to 20 (1 being the highest) in each individual sample, the obtained rankings were averaged for the same age and strain groups, and the table contains the list of ions in each condition with an average of 10 or less. The molecules consistent with the molecular weight of A2E-related compounds are shown in bold and the rightmost column indicates their known chemical structures.

Similar to the individual sample presented above, the summarized information confirms that most of the highly correlating ions were related to A2E. As the majority of these molecules were detected in all the different strains and ages, their identification is highly confident. There were also some differences in the composition of lipofuscin, however, depending on the age and strain of the animals. Water loss from A2E (m/z 574.4) was only observed at high correlation to lipofuscin in *Abca4*$^{-/-}$ mice together with some usually less abundant or higher oxidation states of A2E (m/z 640.3, m/z 688.3, m/z 746.2, or m/z 1223.5). The ion at m/z 733.1 only correlated with lipofuscin in C57Bl6/J animals while heme (m/z 615.9, fragmentation confirmed by MS/MS) as well as higher molecular weight ions (such as m/z 799.3 or ions between m/z 850–1000) only correlated with lipofuscin in *Sv129* mice. Three molecules (m/z 541.8, m/z 650.4 and m/z 656.5) shared a correlation with lipofuscin in both *Sv129* and *Abca4*$^{-/-}$ mice. In regard to age, other highly correlating ions were present in only young (i.e. 2 month old) animals (m/z 698.0 and m/z 806.1) while m/z 650.4 was found to correlate prominently in older mice only.

From the prominent non-A2E peaks in 6 month old *Abca4*$^{-/-}$ mice (m/z 634.4, m/z 650.4, m/z 787.6, and m/z 816.0), m/z 634.4 were found to correlate highly in all the different strains and m/z 816.0 correlated highly in each separate condition (age and strain). Interestingly, the m/z 650.4 ion was not in the list for young mice or in the *C57Bl6/J* animals, and the occurrence of m/z 787.6 with high correlation to lipofuscin was limited to *Abca4*$^{-/-}$ mice. Although the ion m/z 634.4 showed a high correlation to lipofuscin in most samples it was ranked lower for some 6 month *Abca4*$^{-/-}$ tissues, which resulted in its lack

NIH-PA Author Manuscript

NIH-PA Author Manuscript

NIH-PA Author Manuscript

in Tab. 2, however, it was still among the moderately correlating molecules in some individual samples such as the one shown in Fig. 2 and Tab 1.

4. Discussion

The enormous potential impact of a treatment for AMD and the lack of success with other methods [31] has made the inhibition of A2E accumulation a major pharmaceutical target, evidenced by ongoing clinical trials. However, a clear understanding of lipofuscin composition and the identification of its toxic component has not been achieved. Due to the mismatch of spatial fluorescence information (which defines lipofuscin) and the analytical information on its components, the composition of lipofuscin has proven to be an elusive target to define by traditional means of organic tissue analysis. The complexity of the composition of lipofuscin and the highly similar spectral properties of many of its constituent compounds prohibits unequivocal correlation even after painstaking collection of lipofuscin granules under the microscope.

To overcome these difficulties, we have developed a minimally disruptive MALDI-imaging-based technique for the analysis of native RPE tissues. MALDI-IMS provides sensitive and molecularly highly specific imaging information on many molecules in a single experiment. We have successfully utilized this technique to describe the distribution of A2E in both the mouse and human RPE [25, 26, 32]. Furthermore, we have recently demonstrated that determining spatial correlations between lipofuscin fluorescence and the individual images in the MALDI dataset (following a crucial registration procedure) holds a promise for understanding the composition of lipofuscin [27]. Spatial proximity is an essential element of biochemical interactions, thereby, spatial information can be utilized to enhance the detection of biochemically related molecules. Thus, the problem of solving the composition of complex mixtures can become significantly simpler compared to traditional methods of component analysis such as whole-tissue extraction followed by HPLC-MS/MS. Although spatial correlation alone is not sufficient to assert a chemical relationship, the amount of effort required to eliminate false positives is significantly reduced compared to traditional techniques, the output of which is often a confusingly complex mixture of compounds separated according to chemical properties (size, hydrophobicity, etc) while spatial information is lost.

Building on our previous studies, in this manuscript we have determined a small set of lipofuscin components in three mouse models at two different ages in multiple samples each condition. Using four samples in each condition was essential to preclude false positives characteristic of individual samples and achieving a consensus markers for lipofuscin fluorescence. As a further step of validation, the basic findings of this work agree with the results of our previous studies that there is a remarkable correlation between A2E and lipofuscin in the murine RPE [25]. However, the present comprehensive analysis extended our knowledge with the description of more than half a dozen new A2E-related molecules that spatially correlate with lipofuscin. These molecules essentially pinpoint the steps of A2E generation, inter-conversion, and oxidative damage (see Fig. 1).

NIH-PA Author Manuscript

NIH-PA Author Manuscript

NIH-PA Author Manuscript

The abundance of many of these newly identified molecules is too low for simple visual comparison and even a thorough analysis of the mass spectra at numerous arbitrary individual MALDI data points in each tissue is insufficient to unequivocally justify their significance. The implementation of our imaging correlation analysis strategy, however, enhances signals with minimal abundance based on fluorescence information from the same tissue. The power of this technique is that it finds molecular partners with minimal bias. Although it is conceivable that some of these targets could be false positives, using multiple samples can effectively validate these molecules. This strategy allowed the identification of triply- and quadruply-oxidized species of A2E in the samples with highest A2E levels. *In vitro*, using high concentrations of A2E, up to nine oxidations have been detected [33], however, analyzing total mass spectra from the imaging data, previously we have only been able to identify up to two oxidations on A2E in the imaged tissues [25, 32]. With the limited mass resolving power of the utilized MALDI TOF-TOF experiment, some A2E-related compounds (such as phospho-A2E and pentaoxidized-A2E) can potentially overlap. A better separation of the high A2E oxidation levels from phospho-A2E, will require the utilization of FT-ICR-based imaging in the future. Using our approach in multiple samples, we have also managed to identify two novel A2E-related molecules (m/z 634.4 and m/z 650.4, the distributions shown in Figs. 2G–2H) as oxidized and formylated A2E. Interestingly, in organic chemistry formylation is often used to generate oxo compounds in hydrocarbon chains, which is consistent with a biochemical process of increasing oxidation. The detection of these highly oxidized molecules underlines the importance and utility of our fluorescence-enhanced imaging strategy.

In addition to A2E and related molecules, the comprehensive analysis also uncovered various new, age- and strain-specific markers. Heme has been validated by tandem mass spectrometry but the determination of the chemical identities of some of the new targets will require further experimentation. The molecular weight shifts of these ions (m/z 787.6 and m/z 816.0) compared to A2E (+195 amu and +224 amu respectively) do not represent any expected common modifications. As they were situated in a larger lipid cluster of the sample, it is conceivable that they could belong to the envelope of the granules containing lipofuscin.

In summary, the above results have extended previous observations about the dominating presence of A2E-related molecules in mouse lipofuscin and also provided some novel and potentially unrelated lipid molecules that spatially correlate with lipofuscin. The chemical identities of some additional molecules are not yet known, and will need to be described in the future. Nevertheless, these data show that IMS can be utilized as a robust tool for the efficient and comprehensive identification of the components of complex biochemical mixtures. Moreover, the studies demonstrated that connecting clinically relevant diagnostic information (such as fluorescence) with molecularly relevant analytical information can now be successfully accomplished using imaging mass spectrometry.

Supplementary Material

Refer to Web version on PubMed Central for supplementary material.

NIH-PA Author Manuscript

NIH-PA Author Manuscript

NIH-PA Author Manuscript

Acknowledgments

This study is compliant with the recommendations for “Minimum Information About a Proteomics Experiment”. The study was supported in part by NIH grants R21 EY020661 (ZA/RKC), R01 EY004939 (RKC), R01 EY014850 (YK), R01 EY019728 (KS) and R01 EY19065 (ZA); and an unrestricted grant to the Department of Ophthalmology at MUSC from Research to Prevent Blindness (RPB; New York); RKC is an RPB Senior Scientific Investigator. The work has in part been conducted in the MUSC Mass Spectrometry Institutional Research Resource Facility and in the Vanderbilt Mass Spectrometry Research Center.

Abbreviations

A2E	N-retinylidene-N-retinylethanolamine
RPE	retinal pigment epithelium
MALDI-IMS	matrix-assisted laser desorption/ionization imaging mass spectrometry
AMD	age-related macular degeneration

References

1. Nakano M, Oenzil F, Mizuno T, Gotoh S. Age-related changes in the lipofuscin accumulation of brain and heart. Gerontology. 1995; 41:69–80. [PubMed: 8821322]
2. Bajaj NP, Al-Sarraj ST, Anderson V, Kibble M, et al. Cyclin-dependent kinase-5 is associated with lipofuscin in motor neurones in amyotrophic lateral sclerosis. Neurosci Lett. 1998; 245:45–48. [PubMed: 9596352]
3. Hashemzadeh-Bonehi L, Phillips RG, Cairns NJ, Mosaheb S, Thorpe JR. Pin1 protein associates with neuronal lipofuscin: potential consequences in age-related neurodegeneration. Exp Neurol. 2006; 199:328–338. [PubMed: 16480979]
4. Nakanishi H, Amano T, Sastradipura DF, Yoshimine Y, et al. Increased expression of cathepsins E and D in neurons of the aged rat brain and their colocalization with lipofuscin and carboxy-terminal fragments of Alzheimer amyloid precursor protein. J Neurochem. 1997; 68:739–749. [PubMed: 9003065]
5. Ulfig N. Altered lipofuscin pigmentation in the basal nucleus (Meynert) in Parkinson’s disease. Neurosci Res. 1989; 6:456–462. [PubMed: 2771203]
6. Feeney L. Lipofuscin and melanin of human retinal pigment epithelium. Fluorescence, enzyme cytochemical, and ultrastructural studies. Invest Ophthalmol Vis Sci. 1978; 17:583–600. [PubMed: 669890]
7. Wing GL, Blanchard GC, Weiter JJ. The topography and age relationship of lipofuscin concentration in the retinal pigment epithelium. Invest Ophthalmol Vis Sci. 1978; 17:601–607. [PubMed: 669891]
8. Delori FC, Dorey CK, Staurenghi G, Arend O, et al. In vivo fluorescence of the ocular fundus exhibits retinal pigment epithelium lipofuscin characteristics. Invest Ophthalmol Vis Sci. 1995; 36:718–729. [PubMed: 7890502]
9. Davies S, Elliott MH, Floor E, Truscott TG, et al. Photocytotoxicity of lipofuscin in human retinal pigment epithelial cells. Free radical biology & medicine. 2001; 31:256–265. [PubMed: 11440838]
10. Rozanowska M, Korytowski W, Rozanowski B, Skumatz C, et al. Photoreactivity of aged human RPE melanosomes: a comparison with lipofuscin. Invest Ophthalmol Vis Sci. 2002; 43:2088–2096. [PubMed: 12091401]
11. Rozanowska M, Wessels J, Boulton M, Burke JM, et al. Blue light-induced singlet oxygen generation by retinal lipofuscin in non-polar media. Free radical biology & medicine. 1998; 24:1107–1112. [PubMed: 9626564]
12. Sparrow JR, Boulton M. RPE lipofuscin and its role in retinal pathobiology. Experimental eye research. 2005; 80:595–606. [PubMed: 15862166]

NIH-PA Author Manuscript NIH-PA Author Manuscript NIH-PA Author Manuscript

13. Winkler BS, Boulton ME, Gottsch JD, Sternberg P. Oxidative damage and age-related macular degeneration. Molecular vision. 1999; 5:32. [PubMed: 10562656]
14. Ng KP, Gugiu B, Renganathan K, Davies MW, et al. Retinal pigment epithelium lipofuscin proteomics. Mol Cell Proteomics. 2008; 7:1397–1405. [PubMed: 18436525]
15. Sparrow JR, Gregory-Roberts E, Yamamoto K, Blonska A, et al. The bisretinoids of retinal pigment epithelium. Progress in retinal and eye research. 2012; 31:121–135. [PubMed: 22209824]
16. Sparrow JR, Wu Y, Kim CY, Zhou J. Phospholipid meets all-trans-retinal: the making of RPE bisretinoids. J Lipid Res. 2009; 51:247–261. [PubMed: 19666736]
17. Eldred GE, Lasky MR. Retinal age pigments generated by self-assembling lysosomotropic detergents. Nature. 1993; 361:724–726. [PubMed: 8441466]
18. Parish CA, Hashimoto M, Nakanishi K, Dillon J, Sparrow J. Isolation and one-step preparation of A2E and iso-A2E, fluorophores from human retinal pigment epithelium. Proc Natl Acad Sci U S A. 1998; 95:14609–14613. [PubMed: 9843937]
19. Sakai N, Decatur J, Nakanishi K, Eldred GE. Ocular Age Pigment “A2E”: An Unprecedented Pyridinium Bisretinoid. J Am Chem Soc. 1996; 118:1559–1560.
20. Boyer NP, Higbee D, Currin MB, Blakeley LR, et al. Lipofuscin and N-retinylidene-N-retinylethanolamine (A2E) accumulate in retinal pigment epithelium in absence of light exposure: their origin is 11-cis-retinal. The Journal of biological chemistry. 2012; 287:22276–22286. [PubMed: 22570475]
21. Liu J, Itagaki Y, Ben-Shabat S, Nakanishi K, Sparrow JR. The biosynthesis of A2E, a fluorophore of aging retina, involves the formation of the precursor, A2-PE, in the photoreceptor outer segment membrane. J Biol Chem. 2000; 275:29354–29360. [PubMed: 10887199]
22. Mata NL, Weng J, Travis GH. Biosynthesis of a major lipofuscin fluorophore in mice and humans with ABCR-mediated retinal and macular degeneration. Proc Natl Acad Sci USA. 2000; 97:7154–7159. [PubMed: 10852960]
23. Maeda A, Golczak M, Chen Y, Okano K, et al. Primary amines protect against retinal degeneration in mouse models of retinopathies. Nature chemical biology. 2011; 8:170–178.
24. Roberts JE, Kukielczak BM, Hu DN, Miller DS, et al. The role of A2E in prevention or enhancement of light damage in human retinal pigment epithelial cells. Photochem Photobiol. 2002; 75:184–190. [PubMed: 11883606]
25. Grey AC, Crouch RK, Koutalos Y, Schey KL, Ablonczy Z. Spatial localization of A2E in the retinal pigment epithelium. Invest Ophthalmol Vis Sci. 2011; 52:3926–3933. [PubMed: 21357388]
26. Tang PH, Kono M, Koutalos Y, Ablonczy Z, Crouch RK. New insights into retinoid metabolism and cycling within the retina. Progress in retinal and eye research. 2013; 32:48–63. [PubMed: 23063666]
27. Ablonczy Z, Higbee D, Grey AC, Koutalos Y, et al. Similar molecules spatially correlate with lipofuscin and N-retinylidene-N-retinylethanolamine in the mouse but not in the human retinal pigment epithelium. Archives of biochemistry and biophysics. 2013
28. Herrmann KA, Somogyi A, Wysocki VH, Drahos L, Vekey K. Combination of sustained off-resonance irradiation and on-resonance excitation in FT-ICR. Analytical chemistry. 2005; 77:7626–7638. [PubMed: 16316170]
29. Yamamoto K, Yoon KD, Ueda K, Hashimoto M, Sparrow JR. A novel bisretinoid of retina is an adduct on glycerophosphoethanolamine. Invest Ophthalmol Vis Sci. 2011; 52:9084–9090. [PubMed: 22039245]
30. Gutierrez DB, Blakeley L, Goletz PW, Schey KL, et al. Mass spectrometry provides accurate and sensitive quantitation of A2E. Photochemical & photobiological sciences: Official journal of the European Photochemistry Association and the European Society for Photobiology. 2010; 9:1513–1519.
31. Chiou, GCY. Age Related Macular Degeneration: The Recent Advances in Basic Research and Clinical Care. Ying, GS., editor. InTech; Rijeka, Croatia: 2012. p. 283-298.
32. Ablonczy Z, Higbee D, Anderson DM, Dahrouj M, et al. Lack of Correlation Between the Spatial Distribution of A2E and Lipofuscin Fluorescence in the Human Retinal Pigment Epithelium. Invest Ophthalmol Vis Sci. 2013; 54:5535–5542. [PubMed: 23847313]

NIH-PA Author Manuscript

NIH-PA Author Manuscript

NIH-PA Author Manuscript

33. Ben-Shabat S, Itagaki Y, Jockusch S, Sparrow JR, et al. Formation of a nonaoxirane from A2E, a lipofuscin fluorophore related to macular degeneration, and evidence of singlet oxygen involvement. Angewandte Chemie. 2002; 41:814–817. [PubMed: 12491345]

NIH-PA Author Manuscript

NIH-PA Author Manuscript

NIH-PA Author Manuscript

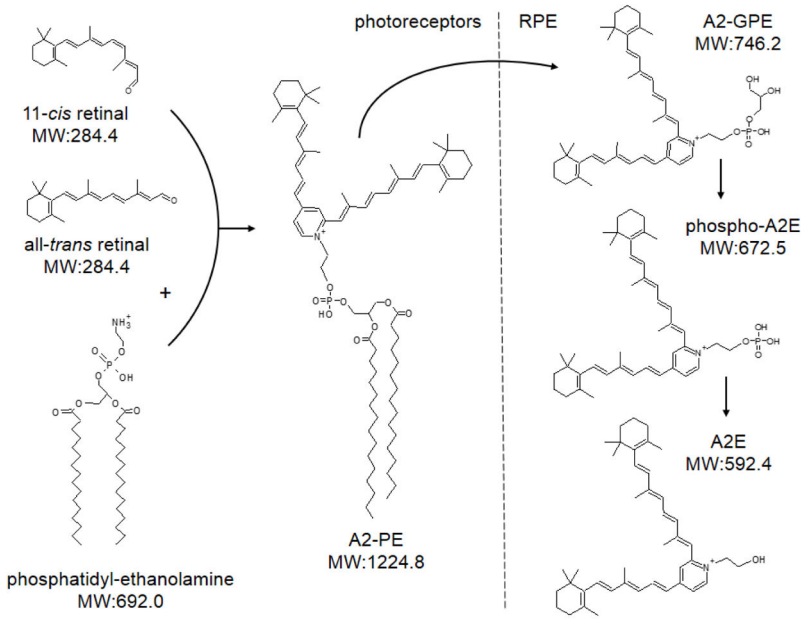

Figure 1. The steps of A2E generation

A2E is derived from the serial interaction of two retinaldehydes (11-*cis* retinal or all-*trans* retinal) with phosphatidyl-ethanolamine in the photoreceptor cells, which generate A2-PE. A2-PE is taken up by the RPE and is degraded by phospholipases into A2E through A2-GPE and phospho-A2E.

NIH-PA Author Manuscript

NIH-PA Author Manuscript

NIH-PA Author Manuscript

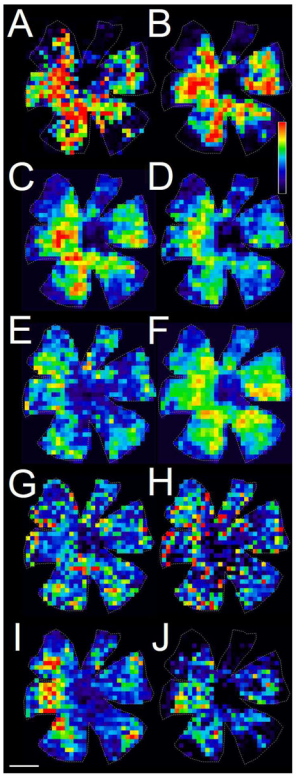

Figure 2. Lipofuscin fluorescence and MALDI images of various molecules in the RPE of a 6 month old Abca4$^{-/-}$ *mouse.*

These molecules showed significant spatial correlation to lipofuscin. The correlation coefficients are summarized in Table 1. (**A**) The distribution of lipofuscin fluorescence (λ_{exc} = 488 nm; λ_{em} = 535 nm). The molecular ions shown are (**B**) m/z 592.4 – A2E; (**C**) m/z 608.4 – singly oxidated A2E; (**D**) m/z 624.4 – doubly oxidated A2E; (**E**) m/z 672.5 – phospho-A2E; (**F**) m/z 746.2 – A2-GPE; (**G**) m/z 634.4 – singly oxidated and formylated A2E; and (**H**) m/z 650.4 – doubly oxidated and formylated A2E. The subsequent molecules also showed high correlation to lipofuscin fluorescence, but they are not thought to be related to A2E: (**I**) m/z 787.6; and (**J**) m/z 816.0. Bar = 1 mm. The intensities are coded by the indicated color scale (0–100%). The images are shown with the resolution of the MALDI imaging dataset.

NIH-PA Author Manuscript

NIH-PA Author Manuscript

NIH-PA Author Manuscript

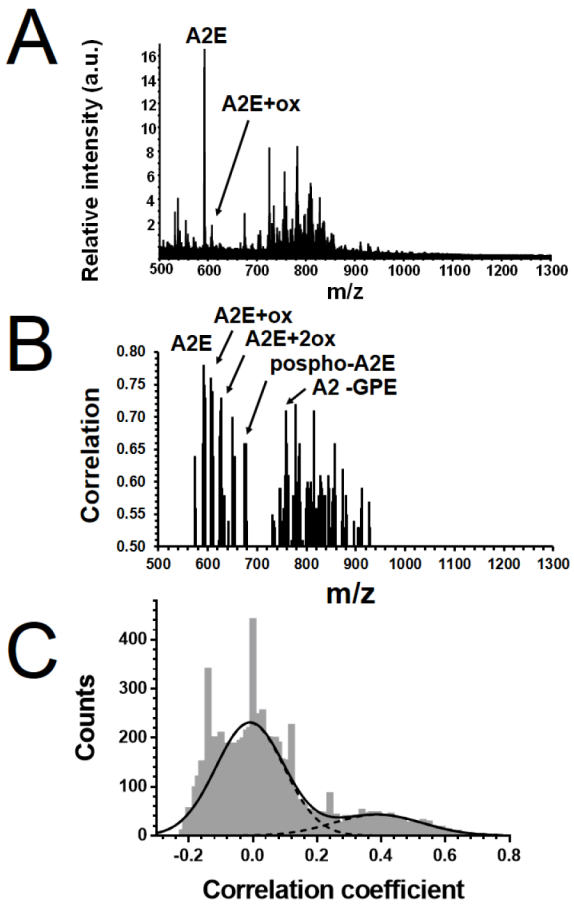

Figure 3. Molecules spatially correlating with lipofuscin in the RPE of a 6 month old Abca4$^{-/-}$ *mouse*

(**A**) Average MALDI mass spectrum (MALDI profile) from the tissue in the m/z 500–1300 range. The spectrum represents the molecules present in the entire dataset. The positions of A2E (m/z 592.4) and singly-oxidized A2E (m/z 608.4) are indicated. (**B**) The array of Pearson correlation coefficients between lipofuscin and every image in the dataset against the corresponding m/z values. The correlations are shown in the m/z 500–1300 range. The positions of A2E (m/z 592.4), singly oxidized A2E (A2E-ox – m/z 608.4); doubly oxidized A2E (A2E-2ox – m/z 624.4); phospho-A2E (m/z 672.5); and A2-GPE (m/z 746.2) are also indicated.

NIH-PA Author Manuscript

NIH-PA Author Manuscript

NIH-PA Author Manuscript

Table 1

The molecular ions with highest correlation to lipofuscin fluorescence in a six month *Abca4*$^{-/-}$ tissue.

MW	ΔMW	R	Slope	Intersect
592.4	0	0.78	1.71	12.06
608.4	16	0.74	12.36	11.55
778.2	186	0.72	54.02	5.64
816.0	224	0.71	17.91	12.53
650.4	58	0.70	140.54	14.81
624.5	32	0.67	31.84	17.22
672.5	80	0.66	115.10	17.60
787.6	195	0.66	27.45	13.49
762.4	170	0.61	21.29	16.86
746.2	154	0.59	19.07	20.34
634.4	42	0.58	70.52	22.61
688.1	96	0.58	70.74	11.90

MW is molecular weight; ΔMW is the shift of the MW compared to A2E, R is the Pearson correlation coefficient. The slope and intersect describe the parameters of the regression analysis.

NIH-PA Author Manuscript NIH-PA Author Manuscript NIH-PA Author Manuscript

Table 2

Summary of the molecular ions with highest correlation to lipofuscin fluorescence.

MW	ΔMW	*C57Bl6/J* 6 month	*Sv129* 2 month	*Sv129* 6 month	*Abca4*$^{-/-}$ 2 month	*Abca4*$^{-/-}$ 6 month	identified compound
522.8	−69				*		
541.8	−50			*	*	*	
574.4	**−18**				*	*	**A2E-H2O**
592.4	**0**	*	*	*	*	*	**A2E**
608.4	**16**	*		*	*	*	**A2E+ox**
615.9	23						heme
624.5	**32**	*		*	*	*	**A2E+2ox**
634.4	42	*		*	*		**formyl-A2E+ox**
640.3	**48**				*		**A2E+3ox**
650.4	58			*		*	**formyl-A2E+2ox**
656.5	**64**			*	*		**A2E+4ox**
672.5	**80**	*	*	*		*	**phospho-A2E**
688.3	**96**				*		**phospho-A2E+ox**
698.0	106		*		*		
704.1	**112**				*		**phospho-A2E+2ox**
715.3	123				*		
733.1	141	*					
746.2	**154**				*	*	**A2-GPE**
762.3	**170**	*	*		*	*	**A2-GPE+ox**
769.5	177					*	
778.5	**186**	*	*	*	*	*	**A2-GPE+2ox**
787.6	195					*	
799.3	207		*				
806.1	214		*		*		
816.0	223	*	*	*	*	*	
828.9	237		*	*	*		
845.0	253	*	*				
856.7	265		*				

NIH-PA Author Manuscript NIH-PA Author Manuscript NIH-PA Author Manuscript

MW	ΔMW	*C57Bl6/J* 6 month	*Sv129* 2 month	*Sv129* 6 month	*Abca4*$^{-/-}$ 2 month	*Abca4*$^{-/-}$ 6 month	identified compound
912.0	320		*				
928.5	336			*			
974.3	382				*		
1015.9	424					*	
1157.1	565		*				
1223.5	**631**				*		**A2-PE**

MW is molecular weight; ΔMW is the shift of the MW compared to A2E. A2E-related molecules are shown in bold. The asterisk indicates that the molecule was highly correlating in the four independent samples per condition.